

---

---

# Longitudinal Amyloid Imaging Using $^{11}\text{C}$ -PiB: Methodologic Considerations

Bart N.M. van Berckel<sup>1</sup>, Rik Ossenkoppele<sup>1,2</sup>, Nelleke Tolboom<sup>1,2</sup>, Maqsood Yaqub<sup>1</sup>, Jessica C. Foster-Dingley<sup>1</sup>, Albert D. Windhorst<sup>1</sup>, Philip Scheltens<sup>2</sup>, Adriaan A. Lammertsma<sup>1</sup>, and Ronald Boellaard<sup>1</sup>

<sup>1</sup>Department of Nuclear Medicine and PET Research, VU University Medical Center, Amsterdam, The Netherlands; and <sup>2</sup>Department of Neurology and Alzheimer Center, VU University Medical Center, Amsterdam, The Netherlands

---

Several methods are in use for analyzing  $^{11}\text{C}$ -Pittsburgh compound-B ( $^{11}\text{C}$ -PiB) data. The objective of this study was to identify the method of choice for measuring longitudinal changes in specific  $^{11}\text{C}$ -PiB binding. **Methods:** Dynamic 90-min  $^{11}\text{C}$ -PiB baseline and follow-up scans (interval,  $30 \pm 5$  mo) were obtained for 7 Alzheimer disease (AD) patients, 11 patients with mild cognitive impairment (MCI), and 11 healthy controls. Parametric images were generated using reference parametric mapping (RPM2), reference Logan values, and standardized uptake value volume ratios (SUVr), the latter for intervals between 60 and 90 ( $\text{SUVr}_{60-90}$ ) and 40 and 60 ( $\text{SUVr}_{40-60}$ ) minutes after injection. In all analyses, cerebellar gray matter was used as a reference region. A global cortical volume of interest was defined using a probability map-based template. Percentage change between baseline and follow-up was derived for all analytic methods. **Results:**  $\text{SUVr}_{60-90}$  and  $\text{SUVr}_{40-60}$  overestimated binding with 13% and 10%, respectively, compared with RPM2. Reference Logan values were on average 6% lower than RPM2. Both SUVr measures showed high intersubject variability. Over time,  $R_1$ , the delivery of tracer to the cortex relative to that to the cerebellum, decreased in AD patients ( $P < 0.05$ ) but not in MCI patients and controls. Simulations showed that SUVr, but not RPM2 and reference Logan values, was highly dependent on uptake period and that changes in SUVr over time were sensitive to changes in flow. **Conclusion:** To reliably assess amyloid binding over time—for example, in drug intervention studies—it is essential to use fully quantitative methods for data acquisition and analysis.

**Key Words:** Alzheimer disease; positron emission tomography;  $^{11}\text{C}$ -Pittsburgh compound-B; receptor parametric mapping; reference Logan; SUVr

**J Nucl Med 2013; 54:1570–1576**  
DOI: 10.2967/jnumed.112.113654

---

**N**europathologically, Alzheimer disease (AD) is characterized by the presence of senile plaques that consist mainly of amyloid- $\beta$  ( $\text{A}\beta$ ) (1). Amyloid burden can be measured in vivo using PET and the ligand *N*-methyl- $^{11}\text{C}$ -2-(4'-methylaminophenyl)-6-hydroxybenzothiazole, also known as Pittsburgh compound-B (PiB) (2).

---

Received Sep. 10, 2012; revision accepted Apr. 19, 2013.  
For correspondence or reprints contact: Bart N.M. van Berckel, Department of Nuclear Medicine and PET Research, VU University Medical Center, P.O. Box 7057, 1007 MB Amsterdam, The Netherlands.  
E-mail: b.berckel@vumc.nl  
Published online Aug. 12, 2013.  
COPYRIGHT © 2013 by the Society of Nuclear Medicine and Molecular Imaging, Inc.

Previous studies using  $^{11}\text{C}$ -PiB have shown high diagnostic accuracy for the detection of AD (2,3). Longitudinal studies, however, have provided inconsistent findings with either no (4–6) or modest (7–9) changes in  $^{11}\text{C}$ -PiB binding over time in AD patients. Apart from other methodologic considerations, one possible explanation for these inconsistent results could be the method used to quantify specific  $^{11}\text{C}$ -PiB binding.

In a previous study, receptor parametric mapping (RPM2, a basis function implementation of the simplified reference tissue model) (10) was identified as the best parametric method for analyzing  $^{11}\text{C}$ -PiB data (11). Compared with other methods, RPM2 was least sensitive to noise and showed the highest contrast. The difference in quantitative performance between RPM2 and reference Logan (12) was small, but RPM2 showed slightly better image quality. SUVr (standardized uptake value ratio; cortical uptake normalized to cerebellar gray matter uptake), however, showed higher variability and poorer image quality.

In most clinical  $^{11}\text{C}$ -PiB studies, SUVr has been used to measure amyloid load (2,6,13). This is understandable because SUVr has numerous advantages, such as computational simplicity, shorter scan duration, and less vulnerability to patient movement. Nevertheless, this method is sensitive to differences in both washin and washout of the tracer between subjects (14). Although SUVr may be acceptable for diagnostic purposes—for example, PiB-positive versus PiB-negative—more accurate quantification methods may be needed for longitudinal studies aimed to measure changes in  $^{11}\text{C}$ -PiB binding over time.

Therefore, the aim of this longitudinal study was to compare the most frequently used methods for the analysis of  $^{11}\text{C}$ -PiB scans (RPM2, reference Logan, and SUVr) in relation to changes in binding over time.

## MATERIALS AND METHODS

### Subjects

Data for 7 AD patients, 11 patients with mild cognitive impairment (MCI), and 11 healthy controls were used (5). All subjects underwent baseline and follow-up  $^{11}\text{C}$ -PiB scans, with an interval of  $30 \pm 5$  mo (range, 24–48 mo). Subjects underwent  $^{11}\text{C}$ -PiB scans within an interval of  $2 \pm 1$  (at baseline) and  $1 \pm 1$  (at follow-up) months of the clinical evaluation. Written informed consent was obtained from all subjects after a complete written and verbal description of the study. The study was approved by the Medical Ethics Review Committee of the VU University Medical Center.

### PET

PET scans were obtained using an ECAT EXACT HR+ scanner (Siemens/CTI), equipped with a neuroinsert to reduce the contribution of scattered photons from outside the field of view of the scanner. This

scanner enables the acquisition of 63 transaxial planes over a 15.5-cm axial field of view, thus allowing the whole brain to be imaged in 1 bed position. The properties of this scanner have been reported elsewhere (15). All subjects received a venous cannula for tracer injection. First, a 10-min transmission scan was obtained in 2-dimensional acquisition mode using 3 retractable rotating  $^{68}\text{Ge}$  line sources. This scan was used to correct the subsequent emission scan for tissue attenuation. Next, a dynamic emission scan in 3-dimensional acquisition mode was started simultaneously with the intravenous injection of  $351 \pm 82$  (baseline) or  $377 \pm 91$  (follow-up) MBq of  $^{11}\text{C}$ -PiB, with specific activities of  $41 \pm 22$  and  $88 \pm 40$  GBq  $\mu\text{mol}^{-1}$ , respectively.  $^{11}\text{C}$ -PiB was injected using an infusion pump (Med-Rad; Beek) at a rate of  $0.8 \text{ mL}\cdot\text{s}^{-1}$ , followed by a flush of 42 mL of saline at  $2.0 \text{ mL}\cdot\text{s}^{-1}$ . The emission scan consisted of 23 frames with progressive increases in frame duration ( $1 \times 15$ ,  $3 \times 5$ ,  $3 \times 10$ ,  $2 \times 30$ ,  $3 \times 60$ ,  $2 \times 150$ ,  $2 \times 300$ , and  $7 \times 600$  s) for a total scan duration of 90 min. Patient motion was restricted with a head holder and monitored by checking the position of the head using laser beams.

### MR Imaging

All subjects underwent a structural MR imaging scan using a 1.5-T Sonata scanner (Siemens Medical Solutions) at baseline and at follow-up (mean interval between PET and MR imaging,  $2 \pm 1$  and  $1 \pm 1$  mo, respectively). The scan protocol included a coronal T1-weighted 3-dimensional MPRAGE (magnetization-prepared rapid acquisition gradient echo) (slice thickness, 1.5 mm; 160 slices; matrix size,  $256 \times 256$ ; voxel size,  $1 \times 1 \times 1.5 \text{ mm}^3$ ; echo time, 3.97 ms; repetition time, 2,700 ms; inversion time, 950 ms; flip angle,  $8^\circ$ ), which was used for coregistration, segmentation, and region-of-interest (ROI) definition.

### Image and Data Analysis

All PET sinograms were corrected for dead time, tissue attenuation using the transmission scan, decay, scatter, and randoms and were reconstructed using a standard filtered backprojection algorithm and a Hanning filter with a cutoff at 0.5 times the Nyquist frequency. A zoom factor of 2 and a matrix size of  $256 \times 256 \times 63$  were used, resulting in a voxel size of  $1.2 \times 1.2 \times 2.4 \text{ mm}^3$  and a spatial resolution of approximately 7 mm full width at half maximum at the center of the field of view. MR images were aligned to corresponding PET images using a mutual information algorithm. Data were further analyzed using PVElab, a software package that uses a probability map based on 35 delineated ROIs that have been validated previously (16). For the evaluation of the different analytic methods, a global cortical ROI was used. This ROI was composed from the volume-weighted average of the orbital frontal, medial inferior frontal, superior frontal, parietal, superior temporal, medial inferior temporal, and entorhinal cortices together with the hippocampus and posterior cingulate.

### Kinetic Analysis

Data were analyzed on a voxel-by-voxel level using RPM2 (17,18), reference Logan values (12), and SUVrs (19). Cerebellar gray matter was used as reference tissue because of its low levels of fibrillar amyloid in AD patients (20).

We applied a simplified reference tissue model with basis lookup function (21), henceforth referred to as RPM2 (11), to the full 90-min dynamic PET data (10). The outcome measure of RPM2,  $\text{BP}_{\text{ND}}$  (non-displaceable binding potential), is a quantitative measure of specific binding. For RPM2, the dynamic scan was first processed using RPM/simplified reference tissue model. This first step provided parametric images of  $R_1$  (the delivery of tracer to the cortex [ $K_1$ ] relative to that to the cerebellum [ $K_1'$ ]),  $\text{BP}_{\text{ND}}$ , and  $k_2'$ . Next, the median value of  $k_2'$  was determined and subsequently fixed in the second run of RPM2 processing of the dynamic scan. Consequently,  $k_2'$  is fixed on an individual scan basis. The parametrically obtained  $\text{BP}_{\text{ND}}$  reflects the

concentration of specifically bound tracer relative to that of free and nonspecifically bound tracer in tissue under equilibrium conditions. Furthermore, parametric maps of relative delivery ( $R_1$ ) were also generated using RPM2. Reference Logan is based on integration of the differential model equations for target and reference regions. The outcome measure DVR (distribution volume ratio) represents the ratio of distribution volumes of the cortex and cerebellum. For reference Logan, we used the implementation published by Logan et al. (12). In this implementation, it is not required to fix  $k_2'$ , and DVR is derived directly as the slope of the linear part of the graphical plot. More information can be found in Yaqub et al. (11) where we described and evaluated the performance of the various parametric methods in detail.  $\text{SUV}_{\text{r}60-90}$  and  $\text{SUV}_{\text{r}40-60}$  are the ratios of tissue concentrations in the cortex and cerebellum, measured in the time frame from 60 to 90 min and from 40 to 60 min after injection, respectively. The global cortical ROI was projected onto the various parametric images. For the present comparison, results obtained using RPM2 were expressed as  $\text{BP}_{\text{ND}} + 1$ , which corresponds to the outcome measures obtained using reference Logan and  $\text{SUV}_{\text{r}}$ . Percentage changes over time within methods for all groups were calculated using percentage change (%) =  $100 \times (\text{follow-up value} - \text{baseline value}) / (\text{baseline value})$ . Next, relative differences between methods for both baseline and follow-up conditions were calculated using relative difference (%) =  $100 \times (\text{method A} - \text{method B}) / \text{method B}$ .

### Simulations

Simulations were performed to assess effects of flow variations on accuracy of  $^{11}\text{C}$ -PiB binding parameters. Parameters, derived from clinical studies (22), were used in combination with a typical plasma input function. For the reference region the following parameters were used: blood volume fraction  $V_{\text{B}}$  (proportion of tissue volume occupied by intravascular blood) = 0.05, together with  $K_1 = 0.32 \text{ mL}\cdot\text{cm}^{-3}\cdot\text{min}^{-1}$ ,  $k_2 = 0.16 \text{ min}^{-1}$ ,  $k_3 = 0.025 \text{ min}^{-1}$ ,  $k_4 = 0.033 \text{ min}^{-1}$ ,  $\text{BP}_{\text{ND}} = 0.76 (=k_3/k_4)$ , and  $V_{\text{T}}$  (volume of distribution) =  $3.5 (=K_1/k_2 \cdot (1 + k_3/k_4))$ . Parameters for a typical AD region were set at  $V_{\text{B}} = 0.05$ ,  $K_1 = 0.32 \text{ mL}\cdot\text{cm}^{-3}\cdot\text{min}^{-1}$ ,  $k_2 = 0.16 \text{ min}^{-1}$ ,  $k_3 = 0.075 \text{ min}^{-1}$ ,  $k_4 = 0.033 \text{ min}^{-1}$ ,  $\text{BP}_{\text{ND}} = 2.25$ , and  $V_{\text{T}} = 6.5$ .

Flow changes were simulated by proportionally changing  $R_1$ , defined as the  $K_1$  ratio between target and reference regions, while keeping the  $K_1/k_2$  ratio constant. In the simulation, a change in flow is simulated by altering  $K_1$  (and  $k_2$ ), thereby assuming no change in first-pass extraction. This simulation reflects a change in flow between reference and cerebral AD regions (i.e., a heterogeneous flow change) at follow-up.  $R_1$  was varied from 0.6 to 1.4. In addition, a second simulation was performed by keeping  $K_1'$  in the reference region constant and only changing  $K_1$  in cerebral AD regions. Both  $K_1$  in cerebral AD and  $K_1'$  in cerebellar reference regions (and proportionally  $k_2$ , keeping  $K_1/k_2$  constant) were varied from  $K_1 = K_1' = 0.19$  to  $0.48 \text{ mL}\cdot\text{cm}^{-3}\cdot\text{min}^{-1}$ .

For all simulations, SUVrs were calculated for several uptake times and with several simulated flow variations. For comparison,  $\text{BP}_{\text{ND}} + 1 (=DVR)$  was obtained using RPM2 and reference Logan applied to the entire simulated 90-min reference and cortical time-activity curves. For all measures (i.e.,  $\text{SUV}_{\text{r}}$ , RPM2, and reference Logan-based  $\text{BP}_{\text{ND}} + 1$ ), percentage bias compared with true or simulated DVR values were determined. In addition, the percentage change in all parameters as a result of both global and heterogeneous  $K_1$  changes was calculated by comparing these values with true or simulated  $\text{BP}_{\text{ND}} + 1$  (that was kept constant at follow-up).

Simulations were performed both with and without adding noise to the time-activity curve, using a noise model according to Yaqub et al. (23). In the case of noisy simulations, 100 time-activity curves per simulation were generated. The average results from  $\text{SUV}_{\text{r}}$ , RPM2, and reference Logan then were evaluated to study the effect of changes in

**TABLE 1**  
Demographic and Clinical Characteristics According to Diagnostic Group

Variable	Diagnostic group		
	Controls ( <i>n</i> = 11)	MCI ( <i>n</i> = 11)	AD ( <i>n</i> = 7)
Age at baseline (y)	66 ± 7	67 ± 7	61 ± 6
Age at follow up (y)	69 ± 7	70 ± 7	64 ± 6
Interval between scans (mo)	30 ± 4	30 ± 6	32 ± 7
MMSE at baseline	29 ± 1	28 ± 2	26 ± 2*
MMSE at follow-up	29 ± 1	26 ± 3	22 ± 5†

\*ANOVA with post hoc least significant difference tests, AD < MCI, *P* = 0.06; AD < controls, *P* < 0.001; MCI < controls, *P* < 0.05.

†ANOVA with post hoc least significant difference tests, AD < MCI, *P* < 0.05; AD < controls, *P* < 0.001; MCI < controls, *P* < 0.01.

MMSE = Mini-mental State Examination.

$R_1$  and  $K_1$ . Noisy simulations showed results near-identical to those obtained without noise. Therefore, results from the simulations without noise will be reported, such that only flow or  $K_1$  effects are illustrated.

### Statistics

Demographic and clinical differences between groups were assessed using ANOVA with post hoc least significant difference tests and age as covariate. At both baseline and follow-up, mean parameter values of  $^{11}\text{C}$ -PiB binding for the different methods were compared using ANOVA with post hoc least significant difference tests and age as covariate. Finally, group differences in  $R_1$  values at baseline and follow-up were examined using ANOVA with adjustment for age.  $R_1$  changes over time within groups were assessed using paired-samples *t* tests. Data are presented as mean ± SD, unless otherwise stated.

### RESULTS

Demographic and clinical characteristics of the 3 diagnostic groups are presented in Table 1. Groups did not differ with respect to age or mean interval between baseline and follow-up.

### Baseline and Follow-up Binding Measures

Significant differences in  $^{11}\text{C}$ -PiB binding between groups, both at baseline and at follow-up, were found with all methods (Table 2). For all subjects together,  $\text{SUV}_{\text{r}60-90}$  was on average 14% and 13% higher at baseline and follow-up, respectively, than corresponding ( $\text{BP}_{\text{ND}} + 1$ ) values obtained with RPM2. For  $\text{SUV}_{\text{r}40-60}$ , these overestimations were 9% and 10% at baseline and follow-up, respectively. Reference Logan values were on average 6% lower than RPM2 values both at baseline and at follow-up.

### Longitudinal Changes in Binding Measures

Percentage changes between baseline and follow-up differed between methods, especially in AD patients (Table 2). Although  $\text{BP}_{\text{ND}} + 1$  (RPM2), DVR (reference Logan), and  $\text{SUV}_{\text{r}40-60}$  were relatively stable ( $0\% \pm 6\%$ ,  $-1\% \pm 5\%$ , and  $0\% \pm 6\%$ , respectively),  $\text{SUV}_{\text{r}60-90}$  decreased with  $4\% \pm 8\%$  in AD patients. Both SUVr measures showed larger variability than RMP2 values, especially at follow-up (Fig. 1). Differences were less pronounced for MCI patients and controls (RPM2:  $6 \pm 7$ ,  $2\% \pm 3\%$ ; reference Logan:  $5 \pm 6$ ,  $2\% \pm 3\%$ ;  $\text{SUV}_{\text{r}60-90}$ :  $8 \pm 9$ ,  $3\% \pm 4\%$ ; and  $\text{SUV}_{\text{r}40-60}$ :

**TABLE 2**  
Binding Values and Percentage Change of  $^{11}\text{C}$ -PiB According to Analytic Method

Method	AD	MCI	Control	All
RPM2 ( $\text{BP}_{\text{ND}} + 1$ )				
Baseline	1.87 ± 0.10	1.39 ± 0.39	1.12 ± 0.27	1.40 ± 0.41
Follow-up	1.86 ± 0.13	1.46 ± 0.39	1.15 ± 0.29	1.44 ± 0.41
Percentage change	-0.3 ± 5.9	5.5 ± 7.4*	1.9 ± 3.2†	2.7 ± 6.0*
Logan DVR				
Baseline	1.70 ± 0.08	1.31 ± 0.32	1.08 ± 0.23	1.32 ± 0.34
Follow-up	1.68 ± 0.10	1.37 ± 0.32	1.11 ± 0.24	1.35 ± 0.33
Percentage change	-1.0 ± 5.2	5.3 ± 6.0‡	2.1 ± 3.5*	2.6 ± 5.4‡
$\text{SUV}_{\text{r}60-90}$				
Baseline	2.16 ± 0.09	1.57 ± 0.52	1.26 ± 0.38	1.59 ± 0.52
Follow-up	2.07 ± 0.22	1.67 ± 0.50	1.29 ± 0.35	1.62 ± 0.49
Percentage change	-4.3 ± 8.6	8.0 ± 9.2‡	2.6 ± 4.2	2.9 ± 8.7
$\text{SUV}_{\text{r}40-60}$				
Baseline	2.02 ± 0.10	1.54 ± 0.46	1.21 ± 0.32	1.53 ± 0.46
Follow-up	2.02 ± 0.19	1.62 ± 0.46	1.28 ± 0.35	1.59 ± 0.46
Percentage change	0.1 ± 6.4	5.5 ± 7.4*	5.8 ± 6.1‡	4.3 ± 6.9‡

Level of significance for percentage change and for differences between baseline and follow-up values: \**P* = 0.06; †*P* = 0.07; ‡*P* < 0.05.

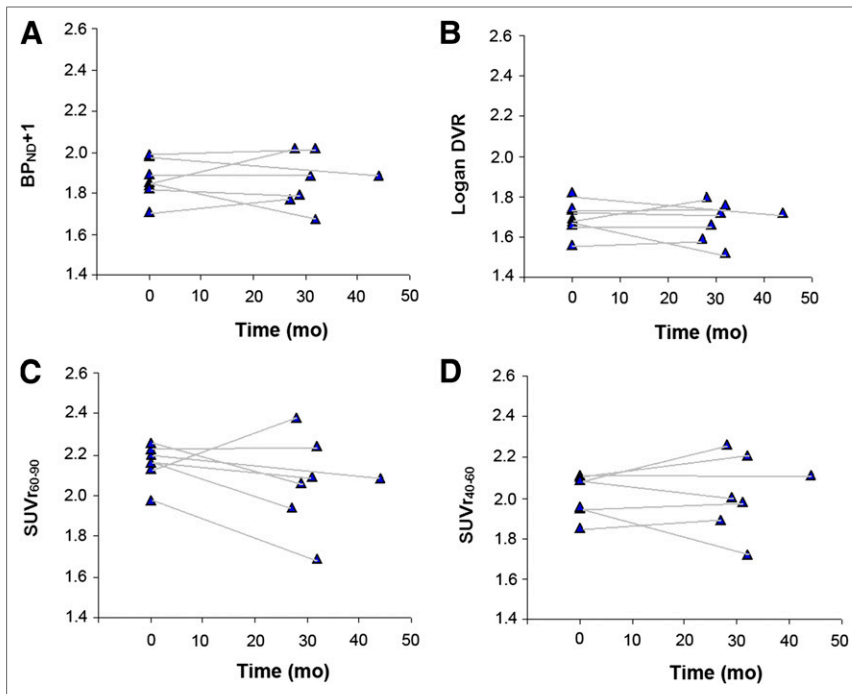


**FIGURE 1.** Global cortical binding of  $^{11}\text{C}$ -PiB in AD patients using RPM2 (A), reference Logan (B),  $\text{SUVr}_{60-90}$  (C), and  $\text{SUVr}_{40-60}$  (D).

$5 \pm 7$ ,  $6\% \pm 6\%$  for MCI and controls, respectively). Parametric images of an AD patient at both baseline and follow-up are presented in Figure 2 for all analytic models.

#### Relative Tracer Delivery

At baseline, mean  $R_1$  values of  $^{11}\text{C}$ -PiB were  $0.87 \pm 0.05$  in patients with AD,  $0.89 \pm 0.03$  in MCI patients, and  $0.87 \pm 0.04$  in controls. At follow-up,  $R_1$  values were  $0.83 \pm 0.06$  in AD patients,  $0.88 \pm 0.03$  in MCI patients, and  $0.88 \pm 0.04$  in controls (Fig. 3).

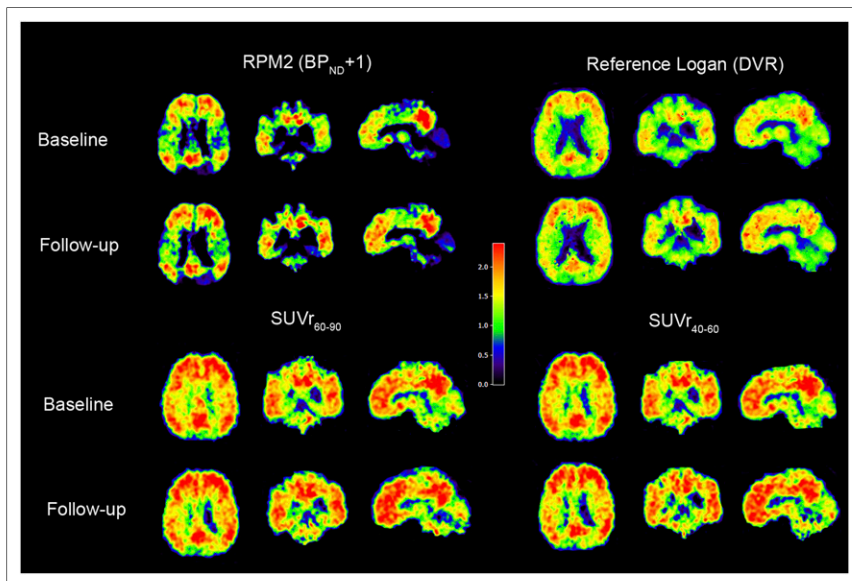


**FIGURE 2.** Parametric images of AD patient with 27 mo of follow-up, showing increased RPM2  $\text{BP}_{\text{ND}} + 1$  (4%), reference Logan DVR (2%), and  $\text{SUVr}_{40-60}$  (2%), whereas  $\text{SUVr}_{60-90}$  decreased with 10%.  $R_1$  was 2% lower at follow-up.

ANOVA adjusted for age revealed no differences in  $R_1$  between groups at baseline ( $F_{(2,28)} = 0.65$ ,  $P = 0.59$ ). At follow-up, however, AD patients showed lower  $R_1$  values than MCI patients and controls at trend level ( $F_{(2,28)} = 2.82$ ,  $P = 0.06$ ) (Fig. 3). Paired-samples  $t$  tests revealed a significant decrease in  $R_1$  over time in AD patients ( $t_{(6)} = 2.85$ ,  $P < 0.05$ ), whereas no changes in  $R_1$  were found for MCI patients ( $t_{(10)} = 1.73$ ,  $P = 0.12$ ) or controls ( $t_{(10)} = 1.03$ ,  $P = 0.33$ ).

#### Simulations

Simulations revealed that  $\text{SUVr}$  was dependent on uptake period (Figs. 4A and 5A). In general,  $\text{SUVr}$  overestimated  $\text{BP}_{\text{ND}} + 1$  (=DVR) for all simulated  $K_1$  variations from 60 min after injection onward. Moreover, changes in both  $K_1$  (global flow changes) and  $R_1$  (heterogeneous flow changes), as shown in Figures 4B and 5B, induced both positive and negative bias in  $\text{SUVr}$  changes when compared with reference (i.e., baseline) conditions ( $K_1 = 0.32 \text{ mL}\cdot\text{cm}^{-3}\cdot\text{min}^{-1}$  and  $R_1 = 1$ , respectively). Bias and flow dependence of  $\text{SUVr}$  were larger than

those of  $\text{BP}_{\text{ND}} + 1$  (RPM2) and DVR (reference Logan), whereas the latter 2 methods showed comparable results.

#### DISCUSSION

This study directly compared changes in  $^{11}\text{C}$ -PiB binding parameters using 4 different analytic methods. It revealed marked differences between methods. Although both kinetic methods (RPM2 and reference Logan) showed relatively stable estimates of  $^{11}\text{C}$ -PiB binding in AD patients over time,  $\text{SUVr}_{60-90}$  demonstrated a decrease in  $^{11}\text{C}$ -PiB uptake. Although this was not observed with  $\text{SUVr}_{40-60}$ , compared with the quantitative methods, both  $\text{SUVr}$  measures showed larger variability between subjects. This variability could be related to changes over time in relative tracer delivery ( $R_1$ ) to the region of interest, because this decreased over time in AD patients.

Both  $\text{SUVr}$  measures overestimated RPM2 values with 9%–14%. Carson et al. (14), using  $^{18}\text{F}$ -cyclofoxy, showed that tissue ratios such as  $\text{SUVr}$ —due to its sensitivity to differences in clearance rate—can overestimate specific binding substantially. In addition, it was shown that this bias was different for high- and low-binding areas. Using  $^{11}\text{C}$ -PiB, Lopresti et al. (19) were the first to describe that  $\text{SUVr}_{40-60}$  and  $\text{SUVr}_{60-90}$  showed a large positive bias, compared with quantitative methods, but that the

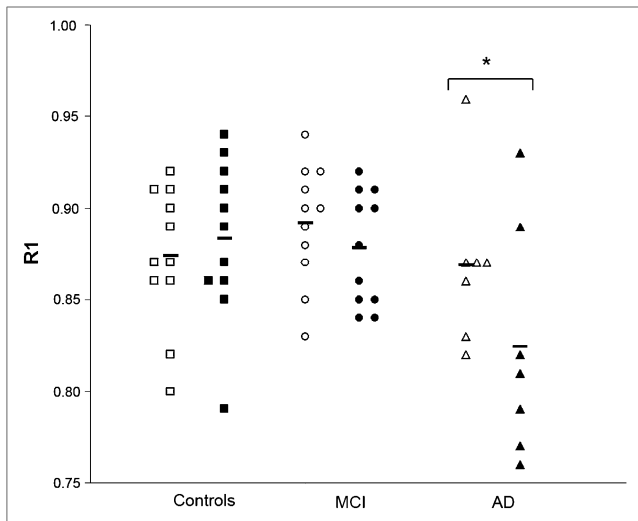


**FIGURE 3.**  $R_1$  values at baseline and follow-up for AD patients ( $\blacktriangle$  and  $\triangle$ ), MCI patients ( $\bullet$  and  $\circ$ ), and controls ( $\blacksquare$  and  $\square$ ). Significant decrease in  $R_1$  was found in AD group only. \* $P < 0.05$ .

percentage bias was fairly similar between low- and high-binding areas. Overestimation of SUVr, compared with quantitative methods, has also been observed using the novel amyloid tracers  $^{18}\text{F}$ -flutemetamol (24) and  $^{18}\text{F}$ -florbetapir (25). Reference Logan estimates were about 6% lower than RPM2 estimates, likely due to the sensitivity of reference Logan graphical analysis to statistical noise (26). In the present study, there was a difference of 17%–19% between SUVr and reference Logan values. In a recent study in MCI patients (27), SUVrs were up to 31% higher than reference Logan DVRs. These discrepancies between methods have important implications for determination of quantitative thresholds for PiB positivity, because these thresholds depend critically on the method that is used to analyze the data.

Both SUVr measures showed larger variability than RPM2 values, especially at follow-up, which can be explained by 2 processes. First, at later time points the SUVr becomes constant over time. Yet, SUVr will overestimate the true DVR as the tissue

curves follow the clearance of plasma input curves. In other words, there is no true equilibrium between plasma concentration and tissue concentration (because the concentration in plasma is lower than in tissue, there will be a net transport of tracer from tissue to plasma). The violation of equilibrium between reference and target regions will be different because of differences in specific binding between these regions and subjects. Because of these differences in nonequilibrium between subjects, there will be more variability of SUVr between subjects. With the performance of dynamic scans and kinetic analysis, the change and variability of the input function (that affects both reference and target region) is considered, and consequently  $\text{BP}_{\text{ND}}$  estimated with RPM2 can be expected to be more reproducible. A second reason may be the variations in flow. To see to what degree the various parametric methods (SUVr, reference Logan, and RPM2) are affected by flow, we performed several simulations. In general, the simulation data were in good agreement with the clinical findings. First, SUVr generally overestimated simulated  $\text{BP}_{\text{ND}} + 1$  (=DVR) values, whereas RPM2 and reference Logan-based values showed minimal bias. Second, these simulations showed that both global and regional (i.e., heterogeneous)  $K_1$  changes over time could result in artificial changes in SUVr over time, a phenomenon that was less prominent for RPM2 or reference Logan. Yet, some small biases and dependence on changes in  $K_1$  were also observed for RPM2 and reference Logan, which can be explained by the contribution of signal from the blood volume fraction. Blood volume fractions were included in the simulations to generate realistic time-activity curves but are, by definition, not considered by both RPM2 and reference Logan. Finally, results obtained using SUVr strongly depended on the specific uptake interval, with slightly less bias and flow dependence for earlier time intervals. This is consistent with clinical data where  $\text{SUVr}_{40-60}$  seemed to show less variability over time than  $\text{SUVr}_{60-90}$ . It is already known that, in AD patients, flow changes over time occur because of disease progression (28), and, consequently, it may be expected that this will result in more variability in SUVr over time. Changes in  $R_1$  seen in AD patients indicate that these flow changes are indeed present. Therefore, it is highly likely that changes in SUVr observed in the present series of AD patients do not reflect changes

in specific  $^{11}\text{C}$ -PiB binding but are rather due to changes in perfusion during the course of the disease. Apart from heterogeneous flow changes (reflected by changes in  $R_1$ ), also relatively large global flow changes are likely to occur both in healthy subjects and in patients. A recent study by Bremner et al. (29) showed that day-to-day variations in global cerebral blood flow were about 30% under normal conditions. As shown by the simulations, these global flow variations could add to the clinically observed variability in SUVr. Similar effects of flow on SUVrs may be expected when using radiotracers other than  $^{11}\text{C}$ -PiB. The flow dependence is caused by the lack of equilibrium of tracer distributions between blood and tissue and the tissue compartments. Therefore this flow dependency occurs for any tracer, although the degree of this effect differs between tracers depending on their kinetic

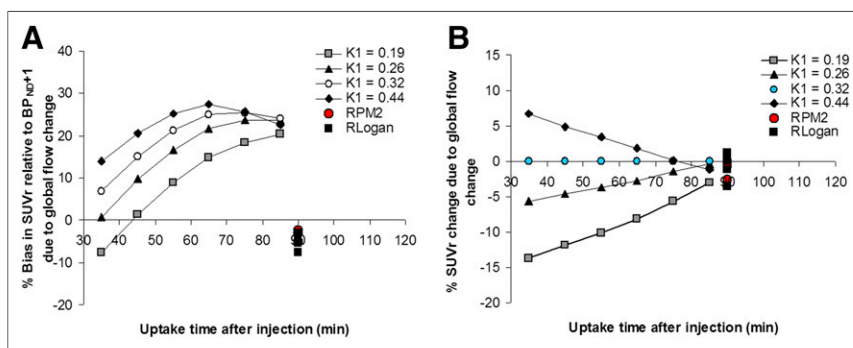


**FIGURE 4.** (A) Percentage bias in SUVr (relative to  $\text{BP}_{\text{ND}} + 1$ ) as function of time for various  $K_1$  values with  $R_1 = 1$  (i.e.,  $K_1 = K_1'$ ). For comparison,  $\text{BP}_{\text{ND}} + 1$  obtained with RPM2 and reference Logan are indicated at 90 min after injection. (B) Percentage bias in change in SUVr (relative to change in  $\text{BP}_{\text{ND}} + 1$ ) as function of time for various follow-up  $K_1$  values, baseline  $K_1 = 0.32 \text{ mL}\cdot\text{cm}^{-3}\cdot\text{min}^{-1}$  and with  $R_1 = 1$  (i.e.,  $K_1 = K_1'$ ) both at baseline and at follow-up. For comparison,  $\text{BP}_{\text{ND}} + 1$  obtained with RPM2 and reference Logan are indicated at 90 min after injection. RPM2 and reference Logan results for all simulated  $K_1$  values are plotted at 90 min after injection. x-axis represents mid-time of 10-min period for calculating SUVr measures.

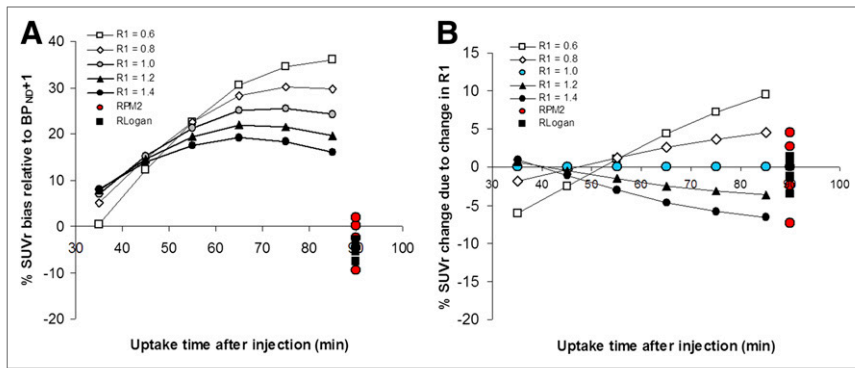


**FIGURE 5.** Regional flow (i.e.,  $K_1$  in simulations) variation effects ( $R_1$ ). (A) Percentage bias in SUVR, compared with true (simulated)  $DVR = BP_{ND} + 1$  as function of uptake time. For comparison, results obtained using RPM2 and reference Logan are indicated at 90 min after injection. (B) Percentage change in SUVR as function of regional flow variation indicating artificial variation in SUVR as result of variations in  $R_1$ . For comparison, results obtained using RPM2 and reference Logan are indicated at 90 min after injection. Small biases are now also observed for RPM2 and reference Logan but with smaller range than those seen with SUVR. RPM2 and reference Logan results for all simulated  $R_1$  values are plotted at 90 min after injection. For both methods, direction of bias (positive or negative) showed same trend as function of  $R_1$  as those seen with SUVR but with smaller amplitudes. x-axis represents mid-time of 10-min period for calculating SUVR measures.

behavior. As such, these findings imply that any study (but particularly when using  $^{11}\text{C}$ -PiB or tracers with similar kinetic behavior) where variations in blood flow can be expected should not be analyzed using SUVR. Consequently, for accurate quantification of longitudinal amyloid imaging studies, dynamic scanning protocols and fully quantitative data analysis methods are essential. This is especially true for longitudinal studies with disease-modifying agents aiming to lower amyloid load in the brain. Studies that use suboptimal methods such as SUVR carry the inherent risk that ineffective drugs are not identified appropriately or, more importantly, that potential effective drugs are dismissed, especially when effect sizes are small. Recently, effects of bapineuzumab on fibrillar amyloid load in AD patients, as measured using  $^{11}\text{C}$ -PiB and PET, were reported (8). This study found a significant reduction in mean  $^{11}\text{C}$ -PiB uptake across 6 targeted ROIs in patients in the treatment arm, compared with those in the placebo group. This is a landmark study, because it was the first, to our knowledge, to show a central effect of a therapeutic approach, aimed at lowering cerebral amyloid load in patients with AD. For the analysis of  $^{11}\text{C}$ -PiB PET scans,  $SUV_{r60-90}$  was used. Results of the present study, however, indicate that  $SUV_{r60-90}$  is susceptible to flow changes, which may be different in bapineuzumab and placebo groups. As such, it is impossible to differentiate between decreases in amyloid load due to treatment and decreases due to flow artifacts. This differentiation is important because potentially, with more stringent methodology, the ineffectiveness of bapineuzumab (30) in the treatment of AD could have been identified in a much earlier phase of development.

One could argue that repeated 90-min dynamic scans cause a selection bias, because only relatively few patients can undergo such a demanding procedure. This is indeed debatable for patients with moderate to severe AD. It is, however, most likely that amyloid-lowering drugs are most effective in the early stages of the disease, justifying inclusion of patients with mild AD or, preferably, prodromal AD or individuals with autosomal dominant AD in a preclinical stage. Dynamic scanning protocols and fully

quantitative data analysis methods are necessary in these patients, as a solid baseline measurement to monitor their disease course and treatment response is needed because it is these patients who will progress to advanced stages with associated blood flow changes. These subjects are perfectly capable of undergoing dynamic scans when carefully prepared and monitored during scanning.

In the case of longitudinal  $^{11}\text{C}$ -PiB studies, a steady-state approach could be an alternative for dynamic scanning (31). Steady-state levels of  $^{11}\text{C}$ -PiB can be achieved using a bolus-with-continuous-infusion protocol, which can be performed outside the PET camera. When a reliable steady state has been achieved, usually a short scanning period is sufficient. This method would combine advantages of a good quantitative measure that is independent of (relative) flow changes with short scan duration. However, this method still needs to be tested and validated for  $^{11}\text{C}$ -PiB.

## CONCLUSION

SUVR should not be used for longitudinal  $^{11}\text{C}$ -PiB studies, especially when only small changes in specific binding can be expected.

## DISCLOSURE

The costs of publication of this article were defrayed in part by the payment of page charges. Therefore, and solely to indicate this fact, this article is hereby marked "advertisement" in accordance with 18 USC section 1734. This work was financially supported by the Internationale Stichting Alzheimer Onderzoek (ISAO, grant 05512) and the American Health Assistance Foundation (AHAF, grant A2005-026). No other potential conflict of interest relevant to this article was reported.

## REFERENCES

- Braak H, Braak E. Neuropathological staging of Alzheimer-related changes. *Acta Neuropathol.* 1991;82:239–259.
- Klunk WE, Engler H, Nordberg A, et al. Imaging brain amyloid in Alzheimer's disease with Pittsburgh Compound-B. *Ann Neurol.* 2004;55:306–319.
- Tolboom N, Yaqub M, van der Flier WM, et al. Detection of Alzheimer pathology in vivo using both  $^{11}\text{C}$ -PiB and  $^{18}\text{F}$ -FDDNP PET. *J Nucl Med.* 2009;50:191–197.
- Engler H, Forsberg A, Almkvist O, et al. Two-year follow-up of amyloid deposition in patients with Alzheimer's disease. *Brain.* 2006;129:2856–2866.
- Ossenkoppele R, Tolboom N, Foster-Dingley JC, et al. Longitudinal imaging of Alzheimer pathology using [ $^{11}\text{C}$ ]PiB, [ $^{18}\text{F}$ ]FDDNP and [ $^{18}\text{F}$ ]FDG PET. *Eur J Nucl Med Mol Imaging.* 2012;39:990–1000.
- Scheinin NM, Aalto S, Koikkalainen J, et al. Follow-up of [ $^{11}\text{C}$ ]PiB uptake and brain volume in patients with Alzheimer disease and controls. *Neurology.* 2009; 73:1186–1192.
- Jack CR Jr, Lowe VJ, Weigand SD, et al. Serial PiB and MR imaging in normal, mild cognitive impairment and Alzheimer's disease: implications for sequence of pathological events in Alzheimer's disease. *Brain.* 2009;132:1355–1365.
- Rinne JO, Brooks DJ, Rossor MN, et al.  $^{11}\text{C}$ -PiB PET assessment of change in fibrillar amyloid-beta load in patients with Alzheimer's disease treated with bapineuzumab: a phase 2, double-blind, placebo-controlled, ascending-dose study. *Lancet Neurol.* 2010;9:363–372.

9. Villain N, Chetelat G, Grassiot B, et al. Regional dynamics of amyloid-beta deposition in healthy elderly, mild cognitive impairment and Alzheimer's disease: a voxelwise PiB-PET longitudinal study. *Brain*. 2012;135:2126–2139.
10. Lammertsma AA, Hume SP. Simplified reference tissue model for PET receptor studies. *Neuroimage*. 1996;4:153–158.
11. Yaqub M, Tolboom N, Boellaard R, et al. Simplified parametric methods for [<sup>11</sup>C]PiB studies. *Neuroimage*. 2008;42:76–86.
12. Logan J, Fowler JS, Volkow ND, Wang GJ, Ding YS, Alexoff DL. Distribution volume ratios without blood sampling from graphical analysis of PET data. *J Cereb Blood Flow Metab*. 1996;16:834–840.
13. Rowe CC, Ellis KA, Rimajova M, et al. Amyloid imaging results from the Australian Imaging, Biomarkers and Lifestyle (AIBL) study of aging. *Neurobiol Aging*. 2010;31:1275–1283.
14. Carson RE, Channing MA, Blasberg RG, et al. Comparison of bolus and infusion methods for receptor quantitation: application to [<sup>18</sup>F]cyclofoxy and positron emission tomography. *J Cereb Blood Flow Metab*. 1993;13:24–42.
15. Brix G, Zaers J, Adam LE, et al. Performance evaluation of a whole-body PET scanner using the NEMA protocol. *J Nucl Med*. 1997;38:1614–1623.
16. Svarer C, Madsen K, Hasselbalch SG, et al. MR-based automatic delineation of volumes of interest in human brain PET images using probability maps. *Neuroimage*. 2005;24:969–979.
17. Gunn RN, Lammertsma AA, Hume SP, Cunningham VJ. Parametric imaging of ligand-receptor binding in PET using a simplified reference region model. *Neuroimage*. 1997;6:279–287.
18. Wu Y, Carson R. Noise reduction in the simplified reference tissue model for neuroreceptor functional imaging. *J Cereb Blood Flow Metab*. 2002;22:1440–1452.
19. Lopresti BJ, Klunk WE, Mathis CA, et al. Simplified quantification of Pittsburgh compound B amyloid imaging PET studies: a comparative analysis. *J Nucl Med*. 2005;46:1959–1972.
20. Yamaguchi H, Hirai S, Morimatsu M, Shoji M, Nakazato Y. Diffuse type of senile plaques in the cerebellum of Alzheimer-type dementia demonstrated by beta protein immunostain. *Acta Neuropathol*. 1989;77:314–319.
21. Koeppe RA, Holden JE, Ip WR. Performance comparison of parameter estimation techniques for the quantification of local cerebral blood flow by dynamic positron computed tomography. *J Cereb Blood Flow Metab*. 1985;5:224–234.
22. Tolboom N, Yaqub M, Boellaard R, et al. Test-retest variability of quantitative [<sup>11</sup>C]PiB studies in Alzheimer's disease. *Eur J Nucl Med Mol Imaging*. 2009;36:1629–1638.
23. Yaqub M, Boellaard R, Kropholler MA, Lammertsma AA. Optimization algorithms and weighting factors for analysis of dynamic PET studies. *Phys Med Biol*. 2006;51:4217–4232.
24. Nelissen N, Van LK, Thurfjell L, et al. Phase 1 study of the Pittsburgh compound B derivative <sup>18</sup>F-flutemetamol in healthy volunteers and patients with probable Alzheimer disease. *J Nucl Med*. 2009;50:1251–1259.
25. Wong DF, Rosenberg PB, Zhou Y, et al. In vivo imaging of amyloid deposition in Alzheimer disease using the radioligand <sup>18</sup>F-AV-45 (florbetapir [corrected] F 18). *J Nucl Med*. 2010;51:913–920.
26. Slifstein M, Laruelle M. Effects of statistical noise on graphic analysis of PET neuroreceptor studies. *J Nucl Med*. 2000;41:2083–2088.
27. Zhou Y, Sojkova J, Resnick SM, Wong DF. Relative equilibrium plot improves graphical analysis and allows bias correction of standardized uptake value ratio in quantitative <sup>11</sup>C-PiB PET studies. *J Nucl Med*. 2012;53:622–628.
28. Alegret M, Cuberas-Borros G, Vinyes-Junque G, et al. A two-year follow-up of cognitive deficits and brain perfusion in mild cognitive impairment and mild Alzheimer's disease. *J Alzheimers Dis*. 2012;30:109–120.
29. Bremmer JP, van Berckel BN, Persoon S, et al. Day-to-day test-retest variability of CBF, CMRO<sub>2</sub>, and OEF measurements using dynamic <sup>15</sup>O PET studies. *Mol Imaging Biol*. 2011;13:759–768.
30. Sperling RA, Salloway S, Raskind M, et al., on behalf of the Bapineuzumab Study 302 Investigators. A randomized, double-blind, placebo-controlled clinical trial of intravenous bapineuzumab in patients with mild to moderate Alzheimer's disease who are apolipoprotein E e4 carriers. [http://www2.kenes.com/efns/info/Documents/Sperling\\_Bapineuzumab%20IV%20Study%20302\\_EFNS%20Presentation%20Slides\\_9-11-2012.pdf](http://www2.kenes.com/efns/info/Documents/Sperling_Bapineuzumab%20IV%20Study%20302_EFNS%20Presentation%20Slides_9-11-2012.pdf). Accessed August 5, 2013.
31. Koeppe RA, Frey KA. Equilibrium analysis of [<sup>11</sup>C]PiB studies. *Neuroimage*. 2008;41:T30.